Laboratory Testing of a Gas Turbine Vaporizer

C. E. Polymeropoulos,* V. Sernas,* and S. Sabadics†
Rutgers University, Piscataway, New Jersey 08855

A laboratory test apparatus was constructed for assessing the metal temperature and the state of different air-fuel mixtures at the outlet of a gas turbine vaporizer fuel injector. The performance of the apparatus was according to the imposed requirements for idle engine operation. Fuels tested were JP5, JP7, and Diesel Fuel Marine. Data consisted of vaporizer metal temperatures, inlet and exit mixture temperatures, as well as power input to the vaporizer. Photographic observations of the exit mixture showed that the liquid phase consisted of droplets, ligaments, as well as irregularly shaped particles originating as pendant droplets around the vaporizer exit. There was no observable difference between the results for JP5 and JP7. The liquid exit temperature, however, for these two fuels appeared to be lower than that for the diesel fuel. The computed extent of vaporization was in qualitative agreement with the experimental observations.

Nomenclature

A = area
C = constant in Eq. (A5)
c_p = specific heat at constant pressure
d = graphite insulation thickness
F_{ij} = configuration factor, or fraction of radiation leaving surface i that is directly intercepted by surface j
F_{kj} = same as F_{ij}
k = thermal conductivity of vaporizer metal
L = latent heat of vaporization
m = mass flow rate
q = rate of heat input
q'' = heat flux
T = absolute temperature
δ = Kronecker delta
ϵ = emissivity
σ = Stefan-Boltzmann constant

Subscripts

a = air
b = base
e = enclosure box, Fig. A1
f = furnace cavity
fu = total fuel flow rate
g = vapor
i = t, f, b, s, r for top, front, base, side, and rear surface, respectively
j = same as i
k = t, f, s, r for top, front, side, and rear surface of the vaporizer, respectively
ℓ = liquid
p = window purge air
r = reference state
v = vaporizer
w = wall or cooling water

Received July 15, 1989; revision received Nov. 20, 1989.

*Professor of Mechanical Engineering, Department of Mechanical and Aerospace Engineering.

†Graduate Student, Department of Mechanical and Aerospace Engineering.

I. Introduction

An alternative to fuel injectors, which break up and atomize the fuel upon introduction into a gas turbine combustion chamber, is a fuel vaporizer. Such devices are aimed at heating the fuel to a sufficiently high temperature so that significant or complete vaporization occurs before combustion. This is accomplished using a fuel injection system consisting of a set of curved vaporizer tubes projecting into the combustion chamber. Through this vaporizer tube, a mixture of compressor air and liquid fuel is introduced into the primary zone. The liquid is supplied at the vaporizing tube entrance at practically combustion chamber pressure, and breakup into particles occurs inside the vaporizer through interaction with the air stream and impaction with the tube walls. Breakup occurs also in the outside shear flow region at the vaporizer exit. The vaporizer tube is exposed to the hot environment of the primary zone and reaches a fairly high temperature through convective and radiative heating. This results in significant fuel vaporization inside the vaporizer so that the exiting mixture consists of liquid, air, and fuel vapor. A description of different types of such vaporizer fuel injection systems and their historical development can be found in Refs. 1-5. The effects of compressor outlet temperature, air to fuel ratio, combustor pressure, and vaporizer tube surface temperature on the extent of vaporization have been qualitatively assessed by Low[6] and Jasuja and Low.[7] The conclusions reached from the previous studies are that both the airstream and the hot walls contribute to fuel vaporization and that the degree of vaporization depends on the engine operating conditions. In fact, for the vaporizing tube to survive the high combustor temperatures, it is probably necessary that a fraction of the fuel remains in liquid form to provide cooling of the tube material. In that respect the name "vaporizer" may be a misnomer, because the device is not expected to provide complete vaporization for all operating conditions. However, in the present work, following previous publications, we will refer to such a fuel injection system as a vaporizer.

Except for some measurements of vaporizer metal temperature using temperature-sensitive paints,[5] obtained using an engine mounted vaporizer, there are no data in the open literature relating fluid and metal temperatures to the overall heat transfer rate and the degree of vaporization, because of the difficulties involved with measurements in a hostile engine environment. The work described in the present paper was the first attempt in obtaining such data for an F402 type-L vaporizer used in the Pegasus engine. The experimental work, which has been described in Ref. 8, involved heating a single vaporizer in a laboratory noncombusting environment and simulat-

Table 1 Vaporizer test conditions for idle operation[a]

Air mass flow rate through vaporizer	5.90×10^{-2} kg/s
Fuel mass flow rate	6.46×10^{-3} kg/s
Vaporizer pressure	186 kPa
Inlet air temperature	372 K
Inlet fuel temperature	Ambient
Maximum vaporizer surface temperature	1000–1153 K
Average vaporizer surface temperature	753–853 K

[a]Furnished by Rolls-Royce, Inc., Atlanta, GA.

ing idle engine operation heat transfer rates. Separate runs using water as the fluid through the vaporizer were used as an aid to heat balance calculations for estimating the degree of vaporization.

II. Experimental Apparatus and Procedure

Table 1 shows experimental conditions required for simulating vaporizer idle operation in the Pegasus engine. Idle conditions were chosen because of the relatively low pressure capability of the experimental equipment used. Laboratory testing under such conditions was carried out using the apparatus and procedure described in the following sections.

A. Vaporizer Test Section

Figure 1 shows a schematic diagram of the vaporizer. Air and liquid fuel entered concentrically, and the resulting mixture exited in the opposing direction after turning through the two 90-deg bends. The inside diameter of the fuel tube and the vaporizer were approximately 0.32 and 2.3 cm, respectively. The distance between the fuel inlet and the centerline of the first bend was approximately 6.8 cm, and the centerline distance between the two bends was 4.8 cm. During engine operation, part of the inlet air is passed through a cooling shroud and is discharged into the combustion chamber. For the present experimentation, however, the shroud air was discharged outside the test chamber by welding shut the annular shroud exit and attaching a separate discharge tube as shown in Fig. 1. The outside wall temperature of the vaporizer was monitored using three type-B (platinum-6% rhodium, platinum-30% rhodium, 0.25-mm-diam wire) grounded thermocouples, T_{v1}–T_{v3}, which were welded on the surface at the locations shown on Fig. 1. T_{v1} monitored the temperature at the vaporizer exit, T_{v2} was located at the position of an expected recirculation region at the first bend, and T_{v3} monitored the temperature at the expected colder underside of the vaporizer. A limited number of experimental runs using an additional thermocouple located at the second bend opposite T_{v2} showed essentially the same temperature as T_{v2}.

Part of the experimentation required observation of the mixture exiting the vaporizer. This was accomplished using a sight tube with windows for still photography using a collimated light beam from a 17 ns pulsed ruby laser. A stream of heated air was used to continuously purge the windows from stray liquid particles, whose presence required masking the viewing area to 0.6×2.3 cm.

The test section pressure was monitored using static pressure taps upstream and downstream of the vaporizer, and the upstream air and fuel temperatures were measured using thermocouples T_{a1} and T_{f1}, respectively, at the vaporizer inlet. A bare thermocouple T_2 was also positioned at the center of the 3.8-cm exhaust tube which was welded on the downstream side of the sight tube as shown in Fig. 1. The significance of temperature readings obtained using a thermocouple junction within a two-phase mixture, such as that exiting the vaporizer, is not clear. To reduce the ambiguity, the thermocouple junction was placed at the center of a shield consisting of a half cylinder, 3 mm in diam and 4 mm long, placed as shown in Fig. 1. It was found that rotating the shield for the concave part to face in the upstream direction did not alter the temperature readings. These thermocouple readings were therefore

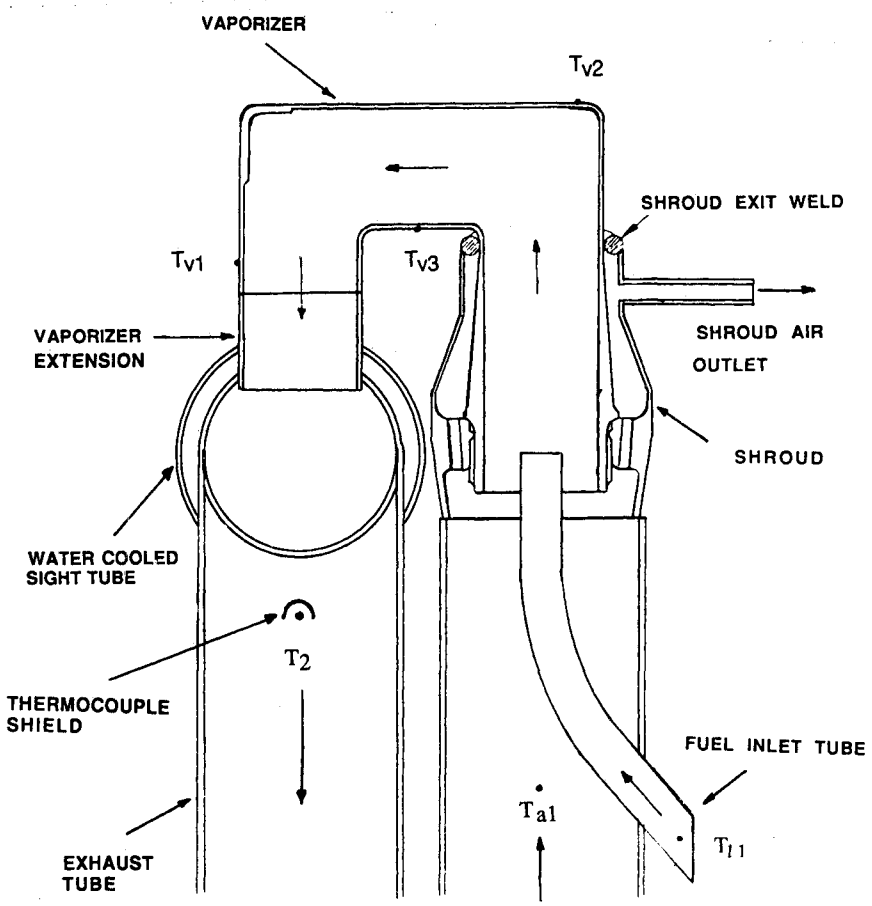

Fig. 1 Schematic diagram of the test section showing thermocouple location.

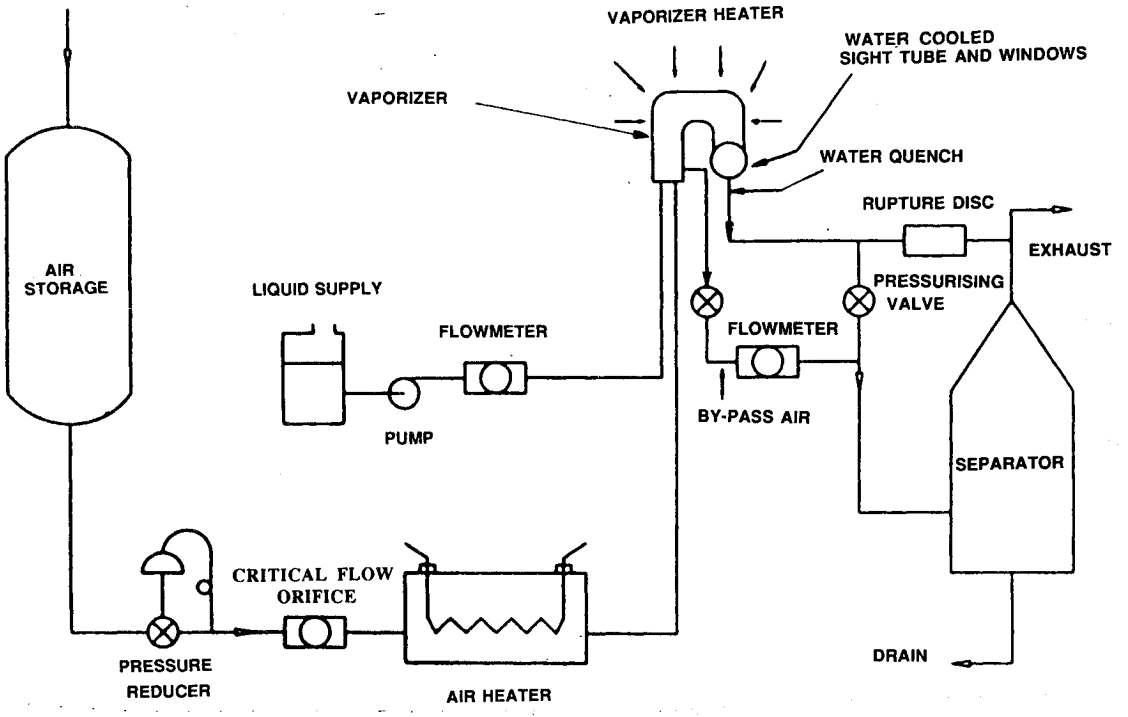

Fig. 2 Flow diagram of the test cell.

considered to represent closely the temperature of the liquid phase (T_{t2}) in the exiting mixture, because under test conditions the half cylinder was presumably filled with liquid that coated the thermocouple junction.

B. Air and Liquid Supply Systems

Figure 2 shows a schematic diagram of the principal components of the air and liquid supply systems. Constant air mass flow rate was maintained using a critical orifice, and the air temperature was controlled electrically. The liquid supply consisted of a separate tank, pump, and flow meter for each fluid. The test section pressure was adjusted using a pressurizing valve, and the mixture leaving the test section was quenched using water injection downstream of the test section. Liquid droplets were separated from the gaseous phase at the exit using the separator shown in Fig. 2. For the present tests, the liquids used were JP5, JP7, Diesel Fuel Marine (DFM) [furnished by the Naval Air Propulsion Center (NAPC), Trenton, New Jersey; JP5 is NAPC fuel no. 9, JP7 is NAPC fuel no. 16, and Diesel Fuel Marine is NAPC fuel no. 17], and water.

C. Vaporizer Heater

Heat addition to the vaporizer was accomplished using radiant heaters arranged to form a heater cavity around the vaporizer as shown schematically in Fig. 3. The heating elements were constructed by cutting 4-mm-thick graphite plates to form continuous flat ribbons approximately 1 cm wide. The plates were supported between graphite posts to form a six-sided enclosure as shown in Fig. 3. The heater plates were 15 cm high, and the total heater area was approximately 800 cm^2. The top of the heater cavity consisted of a sheet of oxidized molybdenum that was electrically insulated from the heaters. A water-cooled, insulated brass rectangular cover was placed over the heater assembly to isolate the heaters from the environment, and for containing the flow of nitrogen gas necessary for maintaining an oxygen-free atmosphere around the graphite heaters. The brass base of the furnace cavity was also insulated and water cooled. Electrical power was provided using a single phase zero angle fired SCR power supply rated at 35 kW. The temperature was monitored using a bare type-B thermocouple placed between the radiant heaters.

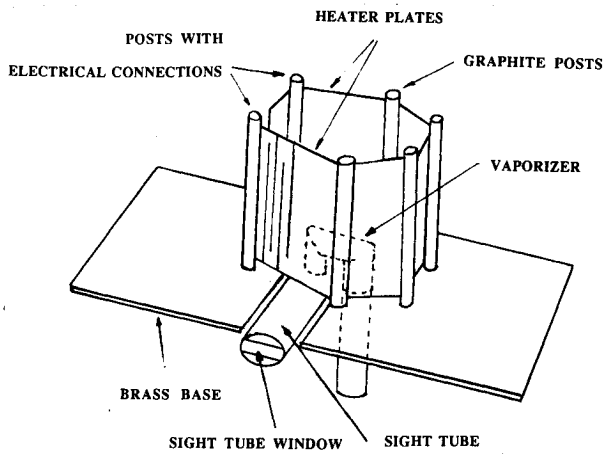

Fig. 3 Schematic diagram of the radiant heater plates in relation to the vaporizer.

D. Experimental Procedure

The experimental procedure consisted of two parts. The first involved operation using water-air mixtures at different water flow rates and various radiant heat inputs to the vaporizer. Using the conditions that resulted in almost complete vaporization, it was then possible to obtain a calibration curve of rate of energy input to the test section as a function of furnace temperature. The second part of the experimentation involved using air-fuel mixtures with the system adjusted to yield conditions shown in Table 1. To provide a common basis of comparison among the fuels tested, the experimentation was carried out for the same rate of vaporizer heat input, which was chosen to yield the vaporizer conditions in Table 1.

III. Experimental Results and Discussion

A. Furnace Calibration Using Water-Air Mixtures

At a given furnace temperature, almost complete vaporization of the liquid water injected could be achieved by reducing its flow rate to a sufficiently low value. This was checked using photographic records of the exiting mixture, such as those

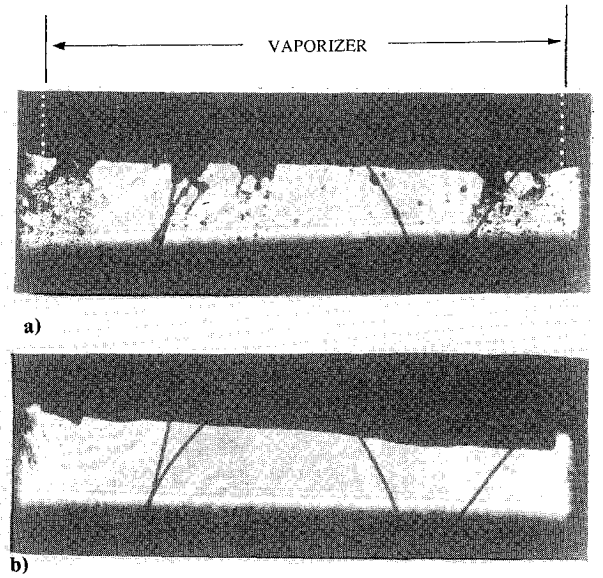

Fig. 4 Vaporizer with air-water mixture flowing: a) $T_{a1} = 372$ K, $m_a = 0.0012$ kg/s, b) $T_v = 646$ K, $T_f = 1663$ K. Flow direction is from top to bottom; vaporizer exit is 2.3 cm in diameter. The four focusing wires are 200 μm in diameter; the distance between each of the two pairs is 7.5 cm in the beam direction. Horizontal interference pattern is due to diffraction from optical masks near the windows.

shown in Figs. 4a and 4b for an unheated and a heated vaporizer, respectively. For completely evaporated mixtures, the outlet thermocouple measures the true mixture temperature. This enables calculation of the energy input to the vaporizer provided the mixture properties are accurately known. For the air-water mixtures employed, Fig. 5 shows the computed rate of energy input plotted against the measured furnace temperature. Within the range of temperatures used, this can be well correlated by the relationship

$$q = 2.3 \times 10^{-13} \times (T_f^4 - T_v^4) \qquad (1)$$

where q (kW) is the rate of radiant energy input to the vaporizer, and T_f, T_v are the furnace and the mean vaporizer temperatures, respectively. Equation (1), which implies radiation from a large enclosure and no convective heat loss, was used to compute the input heat rate to the vaporizer and to set the furnace temperature during subsequent experimentation. Equation (1) was checked analytically by estimating the rate of radiant energy input to the vaporizer. The calculation method is outlined in Appendix A with results that are practically indistinguishable from those predicted by Eq. (1).

B. Temperature Data

Using the experimental apparatus and procedure previously described, a series of tests was carried out using the three fuels, JP5, JP7, and DFM. Results of the principal tests are shown in Table 2, for which the heating rate to the vaporizer was set at approximately 2.5 ± 0.2 kW (obtained by using a furnace temperature around 1863 K). As is shown in Table 2, this resulted in maximum and arithmetic mean vaporizer temperatures that were within the range of values expected in idle operation (see Table 1). Higher temperatures were possible but were avoided because they required conditions that were close to the allowable limit of the type-B thermocouple wire used. Comparison of the JP5 and JP7 temperature results shows no significant difference, although those for the latter fuel appear to indicate slightly higher vaporizer and exit temperatures. The DFM temperature results indicate a significant increase in exit temperature and a slight decrease in vaporizer temperature.

The temperatures in parentheses in Table 2 are estimates of the vaporizer inside surface temperature, and were obtained

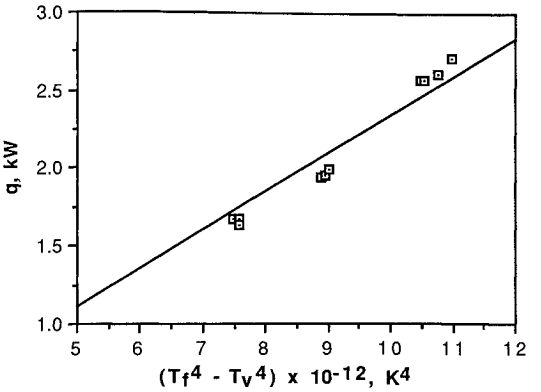

Fig. 5 Rate of energy input of the vaporizer for various furnace operating conditions.

Table 2 Experimental data for idle vaporizer conditions[a]

Fuel	q, kW	Vaporizer temperature, K[b] T_{v1}	T_{v2}	T_{v3}	T_v	T_{a1}	T_{a2}
JP5	2.5	624 (605)	957 (938)	761 (742)	780	372	385
JP7	2.5	631 (612)	971 (952)	782 (737)	794	372	384
Diesel Fuel Marine	2.5	645 (626)	906 (887)	753 (734)	768	372	393

[a]Inlet conditions are those in Table 1.
[b]Numbers in parentheses are computed inside surface temperatures.

using the thickness and mean thermal conductivity of the vaporizer material, the mean heat flux, and the measured mean metal surface temperature. It is interesting to compare these temperatures with approximate distillation ranges for the fuels tested, which are 450–561, 464–517, and 455–616 K for JP5, JP7, and DFM, respectively. The relatively large difference between the metal and distillation end point temperatures suggests that liquid vaporization can be expected for the fuel particles that impinge on the metal. The data in Table 2 also show that the exit temperature T_2 is higher for DFM, which has a higher boiling point range. As previously mentioned, T_2 is probably close to the liquid temperature ($T_{\ell 2}$), which should be expected to increase as the boiling range increases, because the liquid can be heated to a higher temperature before it will evaporate.

The relative magnitude of the measured temperatures T_{v1}, T_{v2}, and T_{v3} can be used to reflect different processes inside and outside the vaporizer. Thus T_{v3} at the underside of the vaporizer tube (see Fig. 1) was the lowest temperature measured because it faced the base plate which was unheated. The highest temperature was registered by T_{v2} on the top surface because it was exposed to the highest heat flux as is shown in Appendix A. In addition, there is the possibility of a recirculating region at the corner where the thermocouple T_{v2} is located. A recirculation region would result in increased fluid temperature as well as heat release due to chemical reaction between the fuel vapor formed in this region and oxygen in the airstream. More definite conclusions in this matter require, however, a larger number of temperature measurements of the vaporizer metal.

C. Photography

Direct photographs of the exiting mixture were taken using the previously described photographic system in order to 1) examine the nature and size of liquid particles and 2) attempt an assessment of the degree of vaporization at the conditions tested. Figures 4a and 4b, which were already mentioned with regard to calibration using water, show the difference in liquid

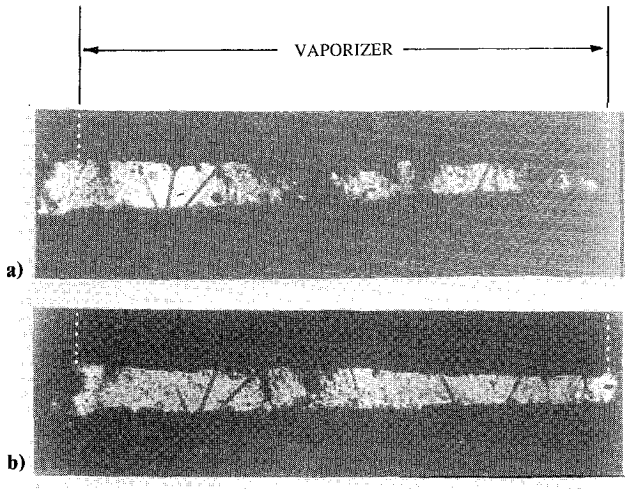

Fig. 6 Vaporizer with: a) JP7-air mixture flowing at conditions shown in Table 1; b) heating as in Table 2. Flow direction, scale, and focusing wires are the same as for Fig. 4.

vaporization between an unheated and a heated vaporizer. Similarly, comparison of Figs. 6a and 6b for JP7 fuel suggests that some vaporization is present, as is evidenced by the reduced number and size of liquid particles. Examination of Figs. 4a, 6a, and 6b shows that the liquid exiting the vaporizer consists of droplets, ligaments, and large irregularly shaped particles. Some of these particles appear to be shed-off liquid pendant drops that form intermittently at the exit lip and are then sheared off by the gas stream, forming ligaments that break down to droplets. It is not possible to quantify or compare the size of these particles for different fuels or operating conditions except in a qualitative fashion. A measure of size and depth of field is given by the four 200-μm-diam focusing wires visible in the photographs. The wires were placed in two pairs and at a distance of 2.5 cm apart in the light beam direction on each side of the vaporizer. The 0.6-cm size of the viewing window in the flow direction was not sufficient to record the complete disintegration process of the liquid.

Photographs of JP5 air mixtures were very similar to those for JP7 in Figs. 6a and 6b. For the case of DFM, however, increasing the vaporizer temperature resulted in complete obscuration of the flowfield at a relatively low rate of heat input to the vaporizer. We believe that obscuration was probably the result of the presence of a large number of very small liquid droplets, which were formed by condensation of the hot fuel vapor (generated from vaporization of the liquid in contact with the vaporizer walls) as it mixed with the colder bulk flow of gas and was cooled below the saturation temperature of the fuel-vapor mixture. Some obscuration was noticed using JP5 and JP7, and none was noticed with water.

D. Extent of Vaporization

Equation (B6), derived in Appendix B, can be used to estimate the limits of vaporization for the experimental conditions tested. Using this equation requires the temperatures of the gas and liquid streams at the vaporizer inlet and exit. As previously discussed, the exit thermocouple temperature T_2 is taken to be the liquid temperature $T_{\ell 2}$. However, the exit gas temperature T_{a2} is not known, thus requiring calculations with this quantity as a parameter. Use of Eq. (B6) also requires the appropriate fluid property relations as well as the heat transfer rate which is computed from Eq. (1). Figure 7 shows results computed for JP7 using data from Table 2, and for water using data corresponding to Fig. 4b. For the purpose of this calculation, there was no appreciable difference between the extent of vaporization of JP7 and JP5. Lack of relevant property information on DFM prevented similar calculations for this fuel.

For each of the two fluids, JP7 and water, Fig. 7 shows the extent of vaporization for different exit gas temperatures but

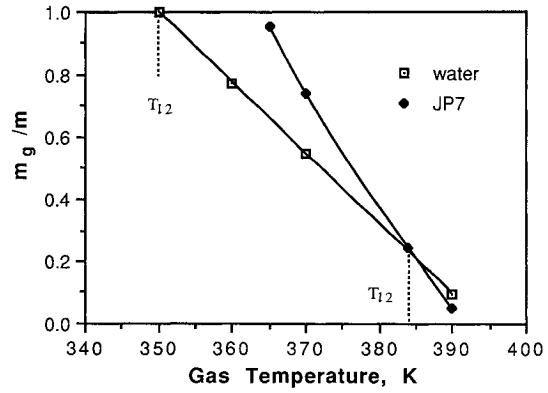

Fig. 7 Extent of vaporization for different gas exit temperatures. Dotted lines show measured liquid exit temperatures.

for fixed exit liquid temperatures, $T_{\ell 2} = T_2$, designated by the dotted lines in the figure. Thus, for water, using an exit liquid temperature of 384 K, the degree of vaporization varied from 0 to 100% as the exit gas temperature changed from approximately 392 to 350 K, meaning that complete vaporization should be expected if the exit gas temperature is near 350 K. This is in agreement with the photographic evidence in Fig. 4b, which shows that for complete vaporization the measured exit liquid temperature was 348 K. Knowledge of the exit stream temperature allows computation of the fraction of energy for liquid heating and vaporization contributed by the vaporizer walls and by the airstream. For the completely vaporized air-water mixture, these were approximately 56 and 44%, respectively, while 80% of this energy was used for the phase change. The large fraction of energy contributed by the airstream accounts for the actual decrease in air temperature across the vaporizer from 372 to 348 K.

The results for JP7 in Fig. 7 were computed for an exit liquid temperature of 384 K, which was equal to the measured value T_2. They show a calculated extent of vaporization from 0 to 100% as the exit gas temperature was varied from approximately 392 to 365 K. A qualitative assessment of the actual exit gas temperature for the JP7 example can be made by comparing the experimentally observed low extent of vaporization evident by the photograph in Fig. 6b with the range of gas temperatures in Fig. 7 that result in low vaporization. Thus, from Fig. 7 for less than 50% vaporization, the exit gas temperature is larger than 375 K, and for less than 25% vaporization, it is larger than 385 K. This leads to the conclusion that for the test conditions in Table 2 for JP7 the gas exit temperature was probably close to or larger than 384 K, which was the temperature measured by the exit thermocouple T_2. Because the inlet air temperature was 372 K, it appears that for this case the air actually increased in net sensible energy across the vaporizer. This is because the boiling point range of JP7 is higher than the inlet air temperature used, allowing for heating of the liquid to a temperature greater than that of the air, followed by heat transfer to the airstream. Additional planned experimentation with higher inlet air temperatures than those used in the present work is expected to provide data on this point.

IV. Conclusions

Experimental apparatus was constructed simulating heat transfer to an F402 vaporizing fuel injector at air and fuel conditions corresponding to near idle operation of the Pegasus engine. The fuels tested were JP5, JP7, and DFM, for which average vaporizer outer metal temperatures recorded were in the range of 768–794 K, with maximum metal temperature in the range of 906–971 K requiring power input in the vicinity of 2.5 kW. The inside surface temperature of the vaporizer was estimated to be considerably higher than the liquid boiling points suggesting significant vaporization of the liquid impinging on the solid surface.

Photographic observation of the exit mixture showed droplets, ligaments, and irregularly shaped particles; however, the size of the viewing windows was not sufficient to record the complete disintegration of the liquid particles. Comparison of the exit stream with and without vaporizer heating showed that, at the conditions tested, there was fuel vaporization present. Estimates of the extent of vaporization were carried out using the exit gas temperature as a parameter. These were also used to set a lower limit on the exit gas temperature for the JP5 and JP7 mixtures tested. At the engine idle air inlet conditions for the three fuels tested, there was negligible net contribution by the airstream to the overall fuel heating process. For air-water mixtures, however, estimates of the fraction of energy transfer to air-water mixtures showed that, for incipient complete vaporization, almost half of the energy required was furnished by the airstream resulting in a gas temperature drop across the vaporizer.

Extension of the present experimental work will include measurements using high inlet air and liquid temperatures with more instrumentation on the vaporizer and the fluid streams. This will provide the basis for more detailed analysis of the heat transfer processes involved.

Appendix A: Radiant Energy Input to the Vaporizer

An assessment of the energy input to the vaporizer is important in order to confirm uniformity of irradiation and also to justify use of Eq. (1) for the experimental determination of the total energy input. For this purpose, a radiant heat exchange analysis was carried out for the combined enclosure consisting of the vaporizer, the heater cavity, and the insulated enclosure box, which are shown schematically in Fig. A1. Specific assumptions to simplify the analysis were as follows:

1) The vaporizer was approximated by an isothermal rectangular parallelepiped with the same height and equivalent overall area (63 cm^2) as the actual vaporizer. The outside surface of the vaporizer exchanged radiant energy with the surfaces and the base of the heater cavity and lost heat by convection to the two phase mixture flowing inside.

2) The graphite heater cavity was also approximated by a rectangular parallelepiped with height equal to the heater height and with sides parallel to the vaporizer (see Fig. A1). The front and top surfaces were assumed to be in radiant balance (consistent with the fact that they were unheated), whereas the rear and two sides were electrically heated and equal in temperature to that recorded by the type-B thermocouple at the center of the heater cavity. The bottom surface of the heater cavity (between the vaporizer and the heater walls) was subject to conduction heat loss because it was part of the enclosure box that was water cooled on the outside.

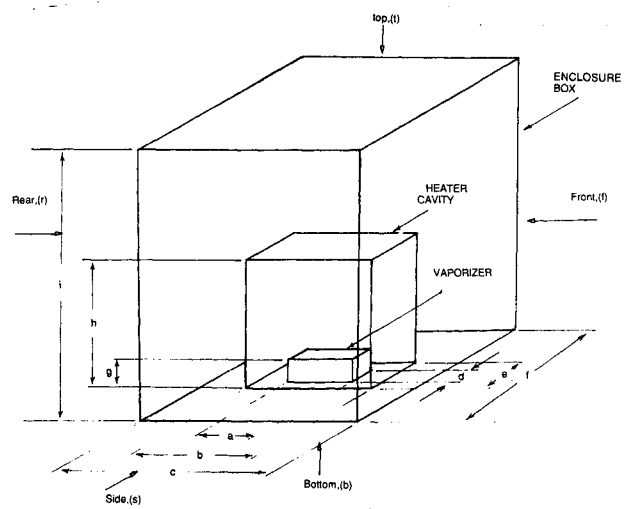

Fig. A1 Schematic diagram of vaporizer, heater cavity, and enclosure box used for radiant energy input estimations. Dimensions in cm are as follows: a = 6.9, b = 14.2, c = 25.0, d = 2.4, e = 5.7, f = 20.0, g = 2.5, h = 14.0, i = 30.0.

3) The ratio of enclosure box area to heater cavity area was approximately 8.3, and the heater was assumed to be located in a large enclosure of equivalent temperature T_e and total area A_e.

4) The inside surface of the enclosure box as well as the base was covered with a layer of graphite insulation approximately 10 mm thick. All surfaces participating in radiation heat exchange, except for the vaporizer, were therefore black.

5) For the purpose of estimating the resulting rate of heat input to the vaporizer, its emissivity was taken to be $\epsilon = 0.8$.

6) Heat exchange by convection was considered negligible compared with that by radiation in view of the low nitrogen flow rate through the heater cavity.

7) The outside surface of the enclosure box was equal to the mean cooling water temperature ($T_w = 340$ K).

8) The heat transfer to the vaporizer was small compared to the total heat generated by the heaters. In the process of computing the temperature of the unheated surfaces of the heater cavity, heat transfer to the vaporizer was therefore neglected.

Subject to the preceding assumptions, the following heat balance can be written for each of the i surfaces of the heater cavity:

$$\Sigma F_{ij}\,(T_i^4 - T_j^4) + (1 - \delta_{ib})(T_i^4 - T_e^4) + \delta_{ib}\,(k/d)(T_b - T_w) = q_i(1 - \delta_{ib})(1 - \delta_{if})(1 - \delta_{it}) \qquad j = t, f, b, s, r \qquad \text{(A1)}$$

where F_{ij} represents the configuration factors, T_i and T_j are the temperatures of surfaces i and j, respectively, q_i is the rate of electrical heat input, δ_{ij} is the Kronecker delta, σ is the Stefan-Boltzmann constant, and k and d are the thermal conductivity and thickness of the graphite insulation at the base surface of the heater. T_b is the base surface temperature, and T_w is the cooling water temperature. The top (t), front (f), and bottom (b) surfaces are in the radiant balance, the bottom surface is losing heat by conduction, and the rear (r) and two side surfaces (s) are heat generating. Except for the bottom surface, the remaining heater surfaces exchange radiant energy with the enclosure box, which is at temperature T_e. The heat transfer between the enclosure box and each of the surfaces of the heater cavity is therefore given by

$$A_e\,(T_e - T_w)(k/d) = \Sigma A_i\,(T_j^4 - T_e^4) \qquad j = t, f, s, r \qquad \text{(A2)}$$

where account is taken of the fact that the bottom surface ($j = b$) of the heater cavity does not see the enclosure box. Equations (A1) and (A2) can be solved for the unknown temperatures T_f, T_r, T_s, T_b, and heat generations q_r and q_s given the geometry (see Fig. A1), the measured water temperature T_w, and the heater temperatures T_s and T_r, which are assumed to be equal to the measured temperature at the center of the heater cavity.

The irradiation q_k'' of each of the vaporizer surfaces is given by the following relation:

$$q_k'' = \sigma\,\Sigma F_{k,j}\,T_j^4 \qquad j = t, f, b, s, r \qquad \text{(A3)}$$

where q_k'' stands for the heat flux to each of the $k = t, f, s, r$ ir-

Table A1 Computed heat transfer to the vaporizer

T_f, K	1860	1760	1660	1560
q_t'', kW/m^2	651	520	410	318
q_s''	493	394	310	240
q_r''	461	369	292	227
q_f''	433	345	271	209
q, kW	2.67	2.13	1.68	1.30
C, kW/K^4 × 10^{13}	2.27	2.27	2.27	2.28

radiated vaporizer surfaces, and $F_{k,j}$ are the angle factors. Finally, the total heat input to the vaporizer is given by

$$q = \epsilon(\Sigma A_k q_k'' - \sigma A_v T_v^4) \quad \text{(A4)}$$

where A_k are each of the vaporizer surfaces, $A_v = \Sigma A_{vk}$, and T_v is the measured mean vaporizer outside surface temperature. To check the validity of Eq. (1), the vaporizer heat input is written as follows:

$$q = C(T_f^4 - T_v^4) \quad \text{(A5)}$$

where C is comparable to the constant in Eq. (1). Table A1 shows the computed irradiation fluxes on each of the vaporizer surfaces q_s'', q_l'', q_f'', q_r''; the total heat input to the vaporizer q; and the value of the constant C for four different heater temperatures T_f corresponding to fluid flow conditions used for Fig. 6.

The results in Table A1 show that Eq. (1) has the correct form, since the constant C does not appear to vary with heater temperature. In addition, they show that the maximum irradiation to the vaporizer occurred at the top surface, which is consistent with what would be expected in an engine environment, where this surface faces the combustion region. In addition, the good agreement between the measured and computed values of C using the reasonable estimate of 0.8 for the emissivity of the vaporizer metal lends credence to the assumptions used in the calculation.

Appendix B: Extent of Vaporization Estimation

A control volume energy balance of the vaporizer involves the following fluid streams: 1) the main heated airstream m_a, which changes temperature between the test section inlet T_{a1} and the exit T_{a2}; 2) the window purge airstream m_p, which changes temperature from the window inlet T_p and exits at T_{a2} after mixing with the main airstream; and 3) the fuel stream m, which enters at temperature T_{f1} and exits as a mixture of vapor m_g at $T_{g2} = T_{a2}$ and liquid m_ℓ at $T_{\ell 2}$.

An energy balance using the measured rate of heat input to the vaporizer q results in the following relation for the fraction of fuel vaporized m_g/m_{fu}:

$$\frac{m_g}{m_{fu}} = \left\{ q + c_{pa}[m_a(T_{a1} - T_{a2}) + m_p(T_p - T_{a2})] - m\int_{T_{f1}}^{T_{\ell 2}} c_{p\ell}\, dT \right\} / D \quad \text{(B6)}$$

where

$$D = \left[L_r + \int_{T_r}^{T_{a2}} c_{pg}\, dT - \int_{T_r}^{T_{\ell 2}} c_{p\ell}\, dT \right] m_{fu}$$

and c_{pa}, c_{pg}, $c_{p\ell}$ are the specific heats at constant pressure for the air, fuel vapor, and liquid fuel, respectively.

The mixing process at the exit requires that $T_{a2} = T_{v2}$. For JP7 the following correlations can be used for the specific heats of the liquid and fuel vapor, respectively[9]:

$$c_{p\ell} = 1.84 + 4.34 \times 10^{-3} \times (T - 273)$$

$$300 < T < 470 \text{ K} \quad \text{(B7)}$$

$$c_{pv} = 1.41 + 0.00414 \times (T - 273)$$

$$300 < T < 570 \text{ K} \quad \text{(B8)}$$

In addition, from Ref. 9, $L_r = 246$ kJ/kg at $T_r = 494$ K. The extent of vaporization using air-water mixtures employed computed data from standard steam tables.[10] Lack of accurate information regarding T_{a2} requires a parametric calculation of the extent of vaporization with this temperature as a variable.

Acknowledgment

This work was performed under subcontract with Rolls-Royce, Inc., Atlanta, Georgia. The Rolls-Royce contract was with the Naval Air Propulsion Center, Trenton, New Jersey.

References

[1]Lindsey, W. H., "The Development of the Armstrong Siddley Mamba Engine," *Journal of the Royal Aeronautical Society*, Vol. 53, No. 1, 1949, p. 137.

[2]Vezhba, I., "Experimental Investigation of Fuel Evaporation in the Vaporizing Elements of Combustion Chambers," NASA TM-75383, 1959.

[3]Alperi, R. W., and Hoffman, J. S., "Liquid Distribution of Low Pressure Drop Injection System-Gas Turbine Vaporizer Design," American Society of Mechanical Engineers, New York, ASME Paper 71-GT-38, 1971.

[4]Parnell, E. C., and Williams, M. R., "A Survey of Annular Vaporizing Combustion Chambers," *Combustion and Heat Transfer in Gas Turbine Systems, Cranfield International Symposium Series*, Vol. 11, Pergamon, London, 1971, p. 91.

[5]Sotheran, A., "The Rolls Royce Annular Vaporizer Combustor," *ASME Transactions, Journal of Engineering for Power*, Vol. 88, 1984, p. 106.

[6]Low, H. C., "Recent Research on the Efflux of the Rolls Royce Vaporizer Fuel Injector," AGARD Conference on Combustor Problems in Turbine Engines, CP 353, Jan. 1984.

[7]Jasuja, A. K., and Low, H. C., "Spray Performance of a Vaporizing Fuel Injector," AGARD Conference on Combustion and Fuels in Gas Turbine Engines, CP 422, June 1988.

[8]Sabadics, S., "Extent of Fuel Vaporization in a Gas Turbine Vaporizer," M.S. Thesis, Rutgers Univ., Piscataway, NJ, 1987.

[9]Coordinating Research Council, "Aviation Fuel Properties," Society of Automotive Engineering, Warrendale, PA, 1988.

[10]Haar, L., and Gallagher, J. S., *NBS/NRC Steam Tables*, Hemisphere, Washington, DC, 1984.